Inhibition of Mitochondrial Clearance and Cu/Zn-SOD Activity Enhance 6-Hydroxydopamine-Induced Neuronal Apoptosis

Sua In · Chang-Won Hong · Boyoung Choi ·
Bong-Geum Jang · Min-Ju Kim

Abstract Parkinson's disease (PD) is a common movement disorder among neurodegenerative diseases, involving neuronal cell death in the substantia nigra of the midbrain. Although mechanisms of cell death in PD have been studied, the exact molecular pathogenesis is still unclear. Here, we explore the relationship between two types of cell death, autophagy and apoptosis, which have been studied separately in parkinsonian mimetic model of 6-hydroxydopamine (6-OHDA). 6-OHDA induced autophagy firstly and then later inhibition of autophagy flux occurred with apoptosis. The apoptosis was prevented by treatment of pan-caspase inhibitor, zVAD-fmk (benzyloxycarbonyl-VAD-fluoromethylketone (zVAD)), or early phase inhibitor of autophagy, 3-methyladenine (3-MA), indicating that autophagic induction was followed by the apoptosis. Interestingly, late step inhibitor of autophagy, bafilomycin A1 (BafA), aggravated 6-OHDA-induced apoptosis. This was associated with mitochondrial abnormality such as the inhibition of damaged mitochondrial clearance and aberrant increase of extracellular oxygen consumption. Furthermore, treatment of BafA did not inhibit 6-OHDA-mediated superoxide formation but strongly reduced the hydrogen peroxide production to below basal levels, indicating failure from superoxide to hydrogen peroxide. These results were accompanied by a lowered expression and activity of copper/zinc superoxide dismutase (Cu/Zn-SOD) but not of manganese SOD (MnSOD) and catalase. Thus, the present study suggests that crosstalk among apoptosis, autophagy, and oxidative stress is a causative factor of 6-OHDA-induced neuronal death and provides a mechanistic understanding of PD pathogenesis.

Keywords 6-Hydroxydopamine · Parkinson's disease · Autophagy · Apoptosis · Reactive oxygen species · Superoxide dismutase

Abbreviations

3-MA	3-Methyladenine
6-OHDA	6-Hydroxydopamine
AnV	Annexin V
BafA	Bafilomycin A1
COXIV	Cytochrome C oxidase subunit IV
DCF-DA	Dichlorodihydrofluorescein diacetate
DHE	Dihydroethidium
DMSO	Dimethylsulfoxide
FACS	Fluorescence-activated cell sorting
GD	Glucose deprivation
LC3	Microtubule-associated protein 1A/1B-light chain 3
LDH	Lactate dehydrogenase
MPTP	1-Methyl-4-phenyl-1,2,3,6-tetrahydropyridine
MTT	3-(4,5-dimethylthiazol-2-yl)-2,5-diphenyltetrazolium bromide
PD	Parkinson's disease
PI	Propidium iodide
ROS	Reactive oxygen species
SOD	Superoxide dismutase
tBID	Truncated BH3-interacting domain death agonist
TNFa	Tumor necrosis factor alpha
zVAD	Benzyloxycarbonyl-VAD-fluoromethylketone

Sua In and Chang-Won Hong contributed equally to this work.

S. In · B. Choi · B.-G. Jang · M.-J. Kim (✉)
Department of Anatomy and Neurobiology, College of Medicine,
Hallym University, 1 Hallymdaehak-gil,
Chuncheon, Gangwon-Do 200-702, South Korea
e-mail: zolim@hallym.ac.kr

C.-W. Hong
Department of Pharmacology, College of Medicine, Hallym
University, Chuncheon, Gangwon-Do 200-702, South Korea

Introduction

Parkinson's disease (PD) is the most common neurodegenerative movement disorder and the second most common neurodegenerative disease, involving symptoms such as resting tremors, rigidity, and bradykinesia. The specific pathology of PD is characterized by the degeneration of dopaminergic neurons in the substantia nigra of the midbrain as a result of the formation of intraneuronal inclusions called Lewy bodies [1, 2]. Although the neuropathological hallmarks of PD are well defined, the underlying molecular cause of dopaminergic neurodegeneration remains unclear. However, several potential mediators of neuronal cell death in PD have been proposed through a number of studies for biochemical processes and molecular mechanisms [3–5]. These include oxidative stress, mitochondrial dysfunction, failure in proteasomal/lysosomal systems, endoplasmic reticulum stress, and inflammation [3–5]. To elucidate the cellular mechanism of dopaminergic neuronal death in the nigrostriatal system, generated models by experimental neurotoxins, including 6-hydroxydopamine (6-OHDA) or 1-methyl-4-phenyl-1,2,3,6-tetrahydropyridine (MPTP), have been applied in vitro and in vivo studies of PD [5, 6]. In particular, 6-OHDA-induced toxicity is a commonly used cellular and animal models for investigating the cellular events associated with oxidative stress and neuronal death in the nigrostriatal system and catecholaminergic cells [7].

Oxidative stress is caused by disturbance in the balance between the generation of reactive oxygen species (ROS) and antioxidant defense. Excessive production of ROS changes pro-oxidant/antioxidant homeostasis of cell and can cause cell death mediated by calcium dysregulation or mitochondrial dysfunction, resulting in activation of the apoptotic cellular signaling [8]. In several forms of neurodegenerative disease including PD, oxidative stress often acts as a major contributing factor of neuronal death by neurotoxin [9]. It is widely considered that 6-OHDA initiates cellular oxidative stress. 6-OHDA, which has a similar molecular structure to dopamine, enters neurons via dopamine transporter and generates intracellular reactive oxygen species (ROS) through autooxidation and inhibition of mitochondrial complex I activity [7]. According to studies using 6-OHDA in a variety of cell lines and primary neuronal cultures suggest that mitochondrial dysfunction and caspase activation are implicated in 6-OHDA-induced neuronal death [10]. However, the relationship between 6-OHDA-induced ROS production and neuronal death is less clearly defined.

According to previous reports, PD pathogenesis is associated with several signaling pathways including apoptosis, autophagy, mitophagy, and so on [4, 6]. These pathways are closely related with upstream or downstream signaling pathway of ROS formation. Thus, many studies have been focused on prevention of ROS-mediated cell death pathways. There is

evidence that apoptosis may be involved in neuronal death in PD through in vitro studies using PD-related neurotoxins, which can generate mitochondrial ROS. For example, in an animal model of PD developed using 6-OHDA, the nigrostriatal neurons are TUNEL positive and display a typical morphology of cells undergoing apoptosis [10, 11]. However, it is still debatable whether neurons die only via apoptosis in PD. Autophagy has been reported to be a mechanism of cell death in PD and dysregulation of autophagy may contribute to the pathogenic process [12]. It has been suggested that parkinsonian neurotoxins, such as 6-OHDA and MPTP, may alter the process of autophagy as well as apoptosis [10–12]. In addition, 6-OHDA-induced mitophagy, another form of autophagy, was reported that 6-OHDA can induce mitophagy via mitochondrial localization of extracellular signal-regulated kinase 2 (ERK2) [13]. In spite of individual reports, the relationship between ROS, apoptosis, autophagy, and mitophagy in neurotoxin-induced neuronal death in PD is still unknown.

In this report, we examined mechanisms through which 6-OHDA induces oxidative stress and subsequent neuronal cell death in the neuroblastoma cell line Neuro2a. We first examined the molecular changes in both caspase-dependent apoptosis and autophagy following treatment of 6-OHDA. We next evaluated the effects of pharmacological inhibition of apoptosis by the pan-caspase inhibitor zVAD-fmk (benzyloxycarbonyl-VAD-fluoromethylketone (zVAD)), or autophagy by either 3-methyladenine (3-MA) or bafilomycin A1 (BafA), on 6-OHDA-induced neuronal death. Interestingly, treatment with these inhibitors altered 6-OHDA-induced ROS formation and the reduction of mitochondrial content. Additionally, for the first time, we have implicated copper/zinc superoxide dismutase (Cu/Zn-SOD) in 6-OHDA-mediated neuronal death. These findings suggest a possible link between apoptosis and autophagy and point to a novel and protective role of Cu/Zn-SOD in 6-OHDA-induced neuronal death.

Methods

Chemicals and Plasmids

6-Hydroxydopamine (6-OHDA), 3-methyladenine (3-MA), dihydroethidium (DHE), 3-(4,5-dimethylthiazol-2-yl)-2,5-diphenyltetrazolium bromide (MTT), propidium iodide (PI), and dichlorodihydrofluorescein diacetate (DCF-DA) were obtained from Sigma (USA). zVAD and bafilomycin A1 (BafA) were purchased from EMD chemicals (USA). Annexin V (AnV) was purchased from Life Technologies (USA). Green fluorescent protein (GFP)-LC3 and mCherry-GFP-LC3 plasmid were previously described [14].

Cell Culture

Neuro2a cells were maintained in Dulbecco's modified Eagle's medium (DMEM, GIBCO, USA) supplemented with 10 % heat-inactivated fetal bovine serum (FBS, GIBCO, USA) and 1× antibiotics with penicillin and streptomycin (GIBCO, USA). Cells were cultured at 37 °C under a humidified 5 % CO_2 atmosphere. Neuro2a cells were seeded on 48- or 6-well plates at densities of 0.8×10^4 cells or 1×10^5 cells per well, respectively. The 6-OHDA treatment was performed 24 h after seeding.

MTT Reduction Assay

To measure MTT reduction in viable cells, the cells were incubated with 1 mg/ml of MTT for 1 h at 37 °C. After the incubation, the medium was removed, and the remaining formazan crystals were dissolved in dimethylsulfoxide (DMSO, Sigma, USA). The dissolved solution was added into a 96-well plate. Finally, the absorbance was measured at 570 nm using Infinite M200 PRO 96-well plate reader (Tecan, Switzerland).

LDH Release Assay

To measure cell membrane integrity through cytosolic lactate dehydrogenase (LDH) release, LDH activity in the media of the cells was assayed using a LDH cytotoxicity detection kit (Takara, Japan). The assay was performed according to the manufacturer's instruction. Briefly, after centrifuging the cultured media, the media with substrate (catalyst and tetrazolium dye) from the kit was added into the 96-well plates, and the plates were kept for 10~30 min in a dark room at room temperature. The absorbance was measured at 492 nm using Infinite M200 PRO 96-well plate reader (Tecan, Switzerland).

Cytosolic Nucleosome Detection

To identify cellular apoptosis, we measured cytosolic nucleosomes in the cells using a Cell Death Detection ELISA PLUS kit, following the manufacturer's instructions, which can detect cytoplasmic histone-associated DNA fragment, a marker of apoptosis, through sandwich ELISA for histone and DNA antibodies (Roche, UK) [15]. Cells (4×10^4) grown in 12-well plates were harvested and re-suspended in lysis buffer. Twenty microliters of the lysate was mixed with anti-histone-biotin, anti-DNA peroxidase antibody, and incubation buffer in a streptavidin-coated 96-well plate. The plate was incubated for 120 min at room temperature. Next, the wells were washed and 2,2′-azino-di[3-ethylbenzthiazalin-sulfonate] (ABTS) substrate solution was added. After a 10-min incubation, the

absorbance was recorded at 492 nm on Infinite M200 PRO 96-well plate reader (Tecan, Switzerland).

Immunoblot Analysis

For protein expression analysis, the cells were seeded on 6-well plates. After the 6-OHDA treatment, the cells were harvested, washed in ice-cold PBS, and lysed using an ice-cold lysis buffer containing 10 mM Tris (pH 7.4), 1 % SDS, 1 mM Na_3VO_4, and a protease inhibitor cocktail (Sigma, USA). Following SDS-PAGE, the proteins were transferred onto PVDF membranes (Millipore, USA). The membranes were blocked in 5 % milk in Tris-buffered saline with Tween-20 (TBST; 20 mM Tris, 137 mM NaCl, 0.1 % Tween 20, pH 7.6). For antibody-based detection, the membranes were incubated with the primary antibody overnight at 4 °C, followed by incubation with the appropriate horseradish peroxidase (HRP)-conjugated secondary antibody for ECL (GE Healthcare, USA) detection. The antibodies were used with anti-poly ADP ribose polymerase (PARP1, 1:1000 dilution, Cell Signaling Technology, USA), anti-procaspase-3 (1:1000, Cell Signaling Technology, USA), anti-cleaved caspase-3 (1:1000, Cell Signaling Technology, USA), anti-p62 (1:30,000, Novus, USA), anti-LC3 (1:1000, Novus, USA), anti-beta-actin (1:5000, Sigma, USA), anti-superoxide dismutase 1 (1:2000, Labfrontier, Korea), anti-manganese-containing SOD (MnSOD, 1:1000, BD bioscience, USA), and anti-catalase (1:1000, Novus, USA). The immunoreactive bands were visualized using an enhanced chemiluminescence system (LAS4000, GE Healthcare). The image analysis program ImageJ (NIH, Bethesda, MD) was used for band intensity analysis. The protein concentrations were determined using the bicinchoninic acid (BCA) assay (Sigma, USA).

ROS Measurement

To measure reactive oxygen species (ROS) production, we used 2,7-dichlorodihydrofluorescein diacetate (DCF-DA) and dihydroethidium (DHE) fluorescent dyes and flow cytometry. DCF-DA is primarily responsible for detecting intracellular H_2O_2, and DHE is sensitive to intracellular superoxide radicals. The cells were treated with 10 μM DCF-DA or DHE in Hanks balanced solution (HBSS) for 30 min at 37 °C in the dark. They were washed in ice-cold phosphate buffer saline (PBS), re-suspended in same buffer, and immediately analyzed by flow cytometry under the FL2 or FL3 filter (FACS caliber, Zeiss, German).

Annexin and PI Double Staining

Cell death was analyzed using annexin V and propidium iodide (PI) double staining and flow cytometry. Before staining, 2×10^5 cells were seeded on 60-mm dishes. After the chemical

treatments, the cells were harvested by trypsinization and stained with annexin V-FITC (BD Biosciences, USA) and PI solution for 30 min at room temperature, according to the manufacturer's instructions. Next, the stained cells were analyzed using flow cytometry under the FL2 and FL3 filters (FACS caliber, Zeiss, German).

SOD Activity Measurement

To measure the intracellular SOD activity, an SOD activity kit was used (Cayman, USA), according to the manufacturer's instructions. The cells were extracted with ice-cold lysis buffer containing 50 mM Tris (pH 8.0), 0.5 % Triton X-100, 137 mM NaCl, 2.7 mM KCl, and 1× protease inhibitor cocktail. After 10 min of incubation, the lysates were centrifuged and the supernatant was collected and aliquoted. Ten micrograms of the lysate was assayed for total SOD activity. For measuring MnSOD activity, 3 mM KCN was added to inhibit Cu/Zn-SOD. Cu/Zn-SOD activity was calculated by subtracting MnSOD activity from total SOD activity. The absorbance was measured at 440 nm using Infinite M200 PRO 96-well plate reader (Tecan, Switzerland).

Catalase Activity Measurement

To measure catalase activity, a catalase activity kit was used (Cayman, USA), according to the manufacturer's instructions. This kit is designed based on the reaction of catalase in the samples with methanol in the presence of H_2O_2, which produces formaldehyde. The lysates were extracted using the same procedure that was used for the SOD activity measurement. Five micrograms of the lysate was assayed for total SOD activity. The formaldehyde produced was measured via analyzing its reaction with the chromogen, 4-amino-3-hydrazino-5-mercapto-1,2,4-triazolehe, by measuring the absorbance of the samples at 540 nm, using Infinite M200 PRO 96-well plate reader (Tecan, Switzerland).

Measurement of Extracellular Oxygen Consumption

To measure extracellular oxygen consumption, MitoXpress-Xtra assay kit was used (Luxcel Bioscience, Ireland), according to the manufacturer's instructions. This kit is designed based on the reaction between oxygen in the media and phosphorescent oxygen-sensitive probes, which can be quenched from the excited state of the dye by oxygen. Cells (0.8×10^4) were grown in 96-well plates and appropriate chemicals were treated. Before the assay, preheated mineral oil was added on top layer of media and the plate was incubated at 37 °C. The fluorescence signal was measured at 380-nm excitation and 650-nm emission with 30-μs delay time and 100-μs gate time using time-resolved mode of fluorometer, Infinite M200 PRO 96-well plate reader (Tecan, Switzerland).

Transfection and Staining of Mitochondria and Lysosome

To visualize GFP-LC3 or mCherry-GFP-LC3, the expression plasmids were transfected into cells using Lipofectamine 2000 Reagent (Invitrogen, USA). The transfected cells were treated with chemicals after 1 day. To measure mitochondrial integrity and lysosomal function, MitoTracker and LysoTracker were used (Invitrogen, USA). MitoTracker Green FM was used for staining of total mitochondria and MitotTracker Red CMXRos was for staining of healthy mitochondria. LysoTracker Red DND-99 was selected among LysoTrackers. Cells (0.8×10^4) were grown in 8-well chamber slides (Nunc, USA) and appropriate chemicals were treated. One hundred molar concentration of Mitotracker and 40 nM of LysoTracker were finally treated for 30 min before visualization. Cell was evaluated under inverted fluorescence microscope (Olympus IX70, USA).

Statistical Analysis

The data are presented as the means±S.E.M., with p-values determined using Student's t test. For multiple comparisons, the analyses were performed with one-way ANOVA followed by Tukey's test. All statistical analyses were calculated using SPSS software.

Results

6-OHDA Induces Autophagy and Caspase-3 Activation in Neuro2a Cells

To investigate 6-OHDA-induced toxicity, Neuro2a neuroblastoma cells were incubated with increasing concentrations of 6-OHDA. The MTT reduction decreased in a dose-dependent manner, and significant effects were observed from 6-OHDA concentrations of 50 μM at 6 h and 25 μM at 18 h (Fig. 1a). To evaluate whether 6-OHDA induced autophagy or apoptosis, we performed an immunoblot analysis. The levels of cleaved caspase-3 and PARP, which are apoptotic markers, most increased in the 50 μM 6-OHDA-treated cells at 18 h (Fig. 1b, d). The conversion of LC3-I to LC3-II, an autophagy marker, was significantly increased in a dose-dependent manner by 6-OHDA at 6 and 18 h (Fig. 1b, c). Based on these results, we used a concentration of 50 μM 6-OHDA for all subsequent experiments.
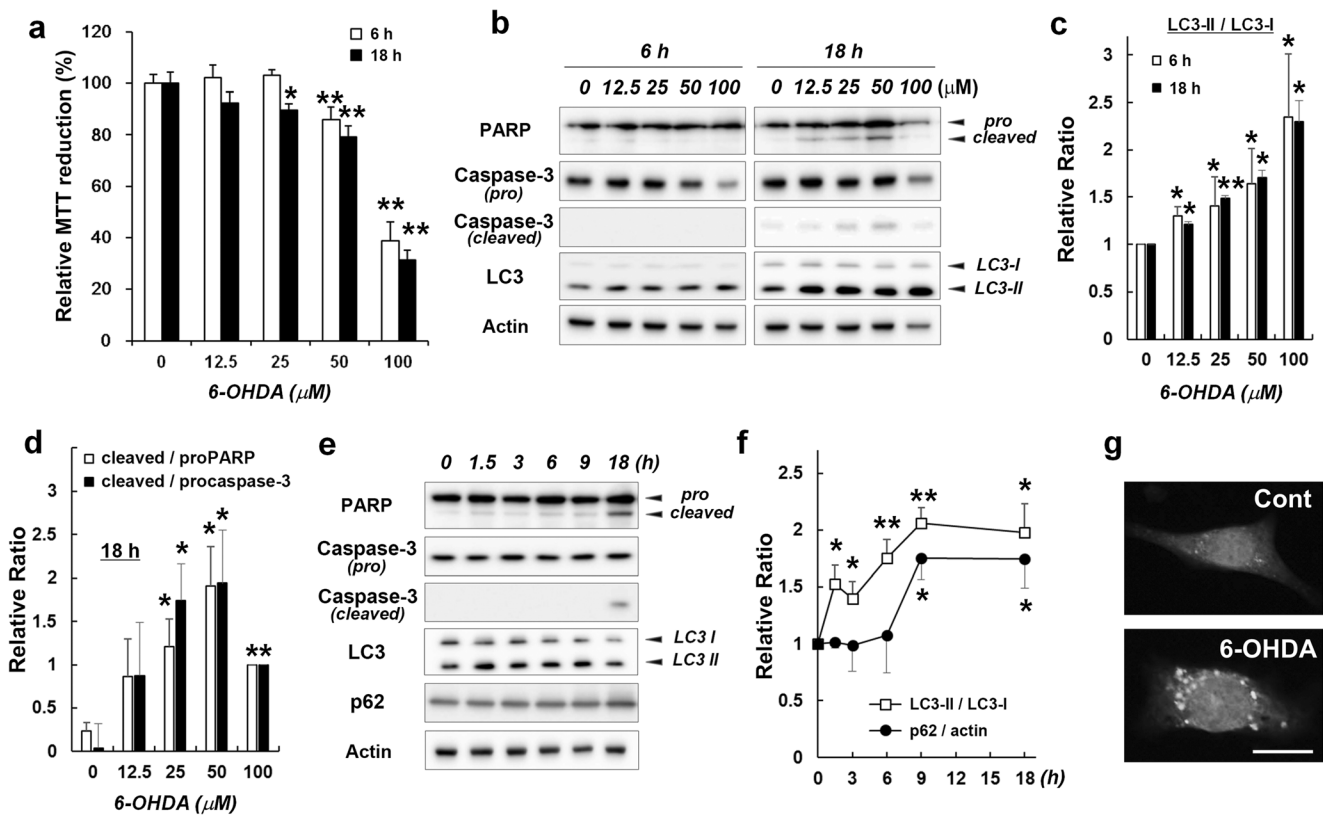
Fig. 1 6-OHDA induced neuronal death and changes in apoptosis and autophagy signals. **a** MTT reduction analysis after treatment with various doses (0~100 μM) of 6-OHDA in Neuro2a cells for 6 and 18 h. **b** Immunoblots of apoptosis (PARP and caspase-3) and autophagy (LC3) markers at 6 and 18 h after the treatment with 6-OHDA. **c, d** The graphs represent relative ratio of each protein from Fig. 1b immunoblots. Densitometry data of LC3-II/LC3-I (**c**) at 6 and 18 h, cleaved/proPARP and cleaved/procaspase-3 at 18 h (**d**). The ratio of each protein was normalized from the untreated control group (**c**) or 100 mM 6-OHDA-treated group (**d**). **e** Immunoblots of apoptosis (PARP and caspase-3) and autophagy (LC3 and p62) markers as time dependency after 50 μM-6-OHDA treatment. **f** Densitometry data of LC3-II/LC3-I and p62/actin from **e**. The ratio was normalized from the group of cells at 0 h. **g** Representative images of fluorescent LC3 *dots*. In Neuro2a cells transiently transfected with GFP-LC3 plasmid, LC3 dots were observed after 50 μM-6-OHDA treatment at 18 h. *Scale bar* represents 10 μm. The graph data are presented as the mean±S.E.M. with *p* values calculated using Student's *t* test (*n*=3). Statistical significance is indicated as *$p<0.05$ and **$p<0.01$ compared with control cells

Next, we examined the time-dependent alterations in the apoptosis and autophagy in response to 6-OHDA. After the 6-OHDA treatment, caspase-3 activation was detected at 18 h and most increased level of cleaved PARP was detected at the same period (Fig. 1e). To access the effect of 6-OHDA on the autophagy flux, we analyzed two biochemical markers of autophagy flux: the conversion of LC3-I to LC3-II and the protein level of p62. Increased autophagic flux is indicated by decreased level of p62 and increased level of LC3-II. Conversely, increased levels of p62 and LC3-II represent decrease of autophagy flux [16, 17]. In this study, treatment of 6-OHDA led significant increase of LC3-II conversion rate from 1.5 h and increased protein level of p62 at 9 h (Fig. 1e, f). Moreover, in Neuro2a cell transient expressing GFP-LC3, treatment of 6-OHDA resulted in the formation of numerous LC3 dots (green) with characterized features of autophagosomes (Fig. 1g). These results suggest that 6-OHDA initially led to autophagy, followed by the decrease

of autophagy flux, and later activated caspase-3-dependent apoptosis.

3-Methyadenine and Bafilomycin A1 Induce Different Responses in Autophagy and Apoptosis Signaling of 6-OHDA-Induced Cell Death

To investigate the detailed relationship between apoptosis and autophagy in 6-OHDA-induced cell death, we examined the effects of a pan-caspase inhibitor (zVAD) and two autophagy inhibitors (3-MA and BafA). In the MTT reduction test, pretreatment of the cells with the inhibitors did not alter the extent of MTT reduction by 6-OHDA, whereas co-treatment with 3-MA decreased and that with BafA increased the MTT value significantly compared to 6-OHDA treatment alone (Fig. 2a). Next, the effects of the inhibitors were analyzed by immunoblotting for apoptosis and autophagy signaling markers (Fig. 2b–d). Immunoblot analysis showed that pretreatment
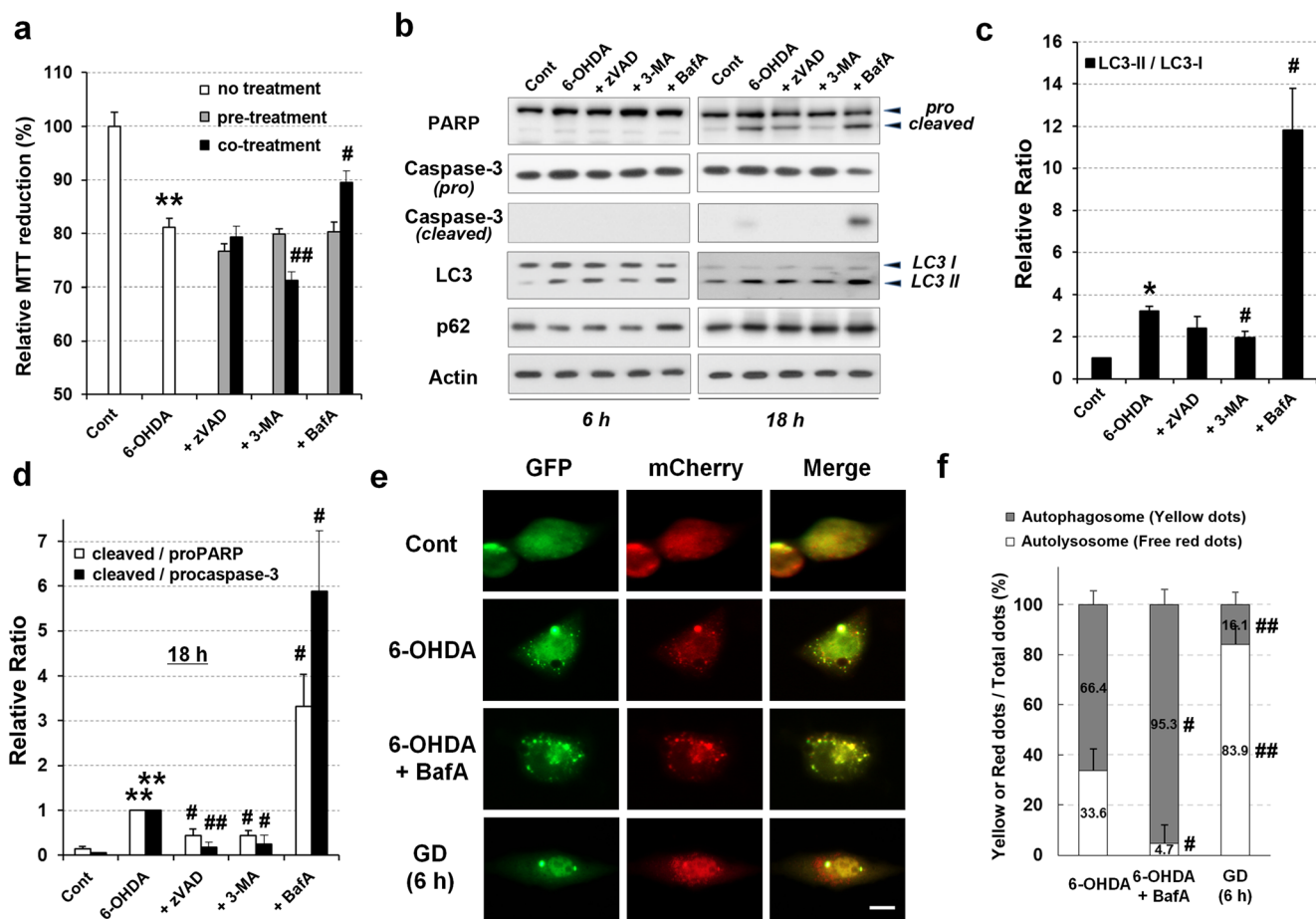
Fig. 2 Effects of apoptosis and autophagy inhibitors on 6-OHDA-induced neuronal death. **a** MTT reduction analysis after treatment of zVAD (100 μM), 3-MA (10 mM), or BafA (20 nM) with 6-OHDA (50 μM). No treatment means treatment of 6-OHDA alone. Pre-treatment with the inhibitors was performed for 1 h and then the inhibitors were removed before the 6-OHDA treatment. Neuro2a cells were co-treated with 6-OHDA and each inhibitor for 18 h. **b** Changes of protein levels by apoptosis and autophagy inhibitors. After co-treatment with 50 μM 6-OHDA and each inhibitor, apoptosis (PARP and caspase-3) and autophagy (LC3 and p62) markers were analyzed by immunoblot at 6 and 18 h. **c, d** Densitometry data for LC3-II/LC3-I (**c**) and cleaved/pro-protein for PARP and procaspase-3 (**d**) from **b** at 18 h. The ratio was normalized from the untreated (**c**) or the cells treated with 6-OHDA alone

(**d**). **e** Representative images of fluorescent LC3 dots. Neuro2a cells were transfected with mCherry-GFP-LC3 and then incubated in 6-OHDA or 6-OHDA + BafA for 18 h. *GD* means glucose deprivation and the transfected cells were exposed to GD for 6 h. *Scale bar* represents 10 μm. **f** Quantitation graph of fluorescence LC3 dots. In merged images, *yellow dots* represent autophagosomes and *red dots* represent autolysosomes per cell (*n*=15 cells per each condition). Indicated values represented by mean % of total dots from two independent experiments. The graph data are presented as the mean±S.E.M. with *p* values calculated using one-way ANOVA with Tukey post-hoc analysis (*n*=3). Statistical significance is indicated as *p<0.05 and **p<0.01 compared with the untreated control and #*p*<0.05 and ##*p*<0.01 compared with the cells treated with 6-OHDA alone

of inhibitors had no significant effect (*data not shown*). Co-treatment of zVAD or 3-MA with 6-OHDA for 18 h decreased the levels of cleaved caspase-3 and PARP. In contrast, co-treatment with BafA strongly increased the levels of cleaved caspase-3 and PARP at 18 h (Fig. 2b, c). Moreover, the accumulation of LC3-II and p62 after treatment with BafA was significantly increased compared to 6-OHDA alone. Treatment of 3-MA with 6-OHDA inhibited the conversion of LC3-I to LC3-II; however, zVAD did not change this conversion compared to 6-OHDA alone (Fig. 2b, d).

To evaluate effects of BafA on autophagy flux, we analyzed changes of autophagosome and autolysosome after treatment with BafA using tandem fluorescent mCherry-

GFP-LC3. mCherry fluorescent (red) is stable in acidic environment such as lysosome whereas GFP fluorescent (green) is acid-labile fluorescent. Thus, green and yellow dots in merged images indicate autophagosomes, and free red dots that do not overlay with green dots indicate autolysosomes [16, 17]. The number of red and their co-localized yellow dots were strongly increased by treatment of 6-OHDA compared to control (Fig. 2f, g). Treatment with BafA significantly increased yellow dots (autophagosomes) and decreased free red dots in merged image compared to 6-OHDA alone (Fig. 2f, g). Traditionally, nutrients starvation such as glucose deprivation (GD) is known for powerful inducing factor of autophagy flux. Thus, we used GD model as a positive control, and the

numbers of free red dots were significantly higher after GD indicating increased autolysosomes.

From these results, autophagy inhibitor in early period, 3-MA, inhibited caspase-3 activation as well as LC3-II conversion, but pan-caspase inhibitor, zVAD, did not affect the levels of LC3-II. Together with the findings of immunoblot analysis in Fig. 1e and Fig. 2b, these results indicated that autophagy was induced before apoptosis activation in 6-OHDA-induced cell death. On the other hand, the other autophagy inhibitor in late stage, BafA, exacerbated the 6-OHDA-induced decrease of the autophagy flux and apoptosis. However, because BafA co-treatment increase the MTT reduction compared with 6-OHDA alone, we next accessed other cell death parameters.

3-Methyadenine Reduces but Bafilomycin A1 Enhances the Cell Death of 6-OHDA-Treated Cells

To evaluate the discrepancy between the results of the MTT test and the immunoblots, we checked the effects of apoptosis and autophagy inhibitors on several parameters of cell death, including cytosolic lactate dehydrogenase (LDH) release into the media, cytosolic nucleosome location, and annexin V (AnV)/propidium iodide (PI) staining measured by flow cytometry. At 18 h, LDH release was significantly decreased by treatment with zVAD or 3-MA, but treatment with BafA increased LDH release compared to 6-OHDA alone (Fig. 3a). Because LDH release is a simple method based on membrane integrity, we next examined cytosolic nucleosome level using ELISA by detecting cytosolic histone and DNA, a hallmark of apoptosis. Induction of cytosolic nucleosome in 6-OHDA-treated cells was inhibited by treatment of zVAD or 3-MA, but not by BafA (Fig. 3b).

Finally, we performed fluorescence-activated cell sorting (FACS) analysis using AnV and propidium iodide (PI). Early stages of apoptosis involve externalization of phosphatidyl-serine (PS), as detected by AnV binding (AnV$^+$) and necrotic or late apoptotic stage having lost membrane permeability and cellular integrity was detected by PI, cell permeable fluorescent dye
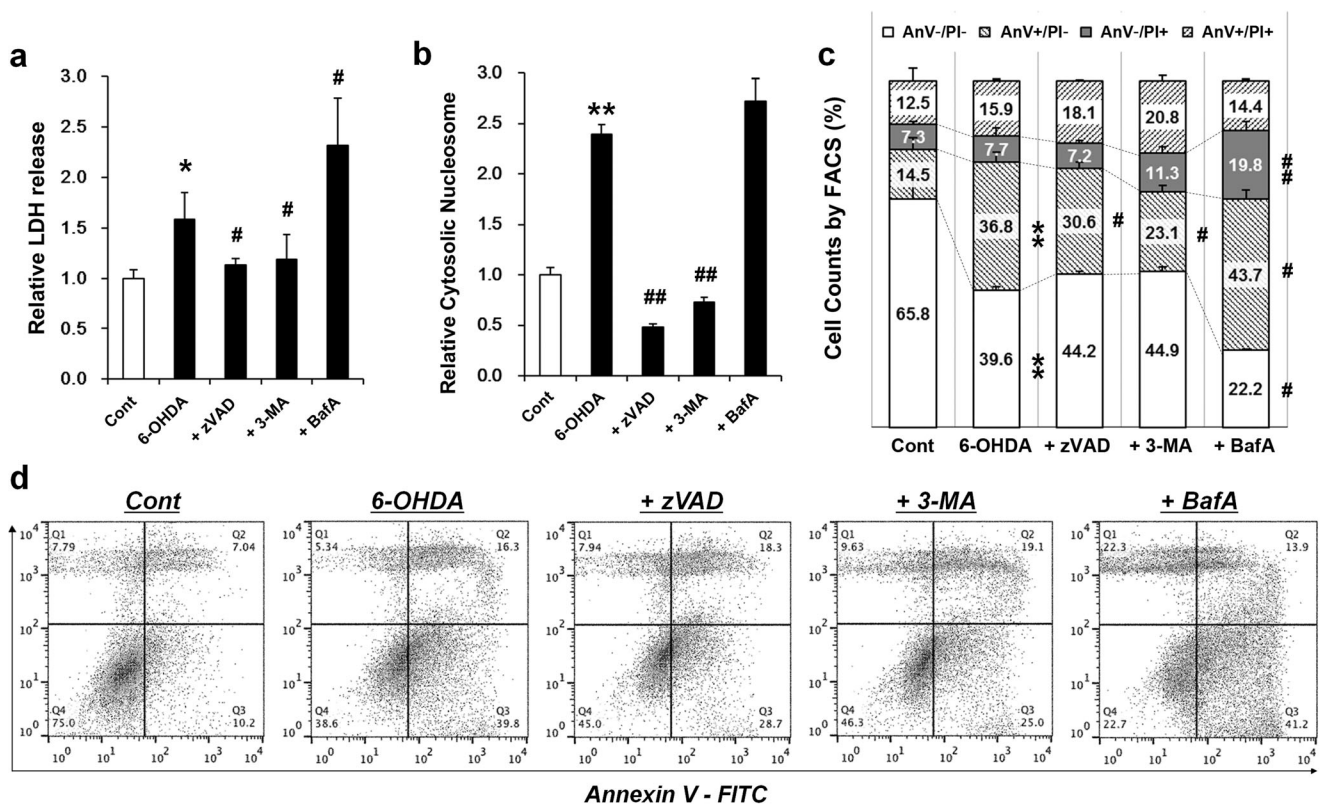

Fig. 3 Change of several cell death parameters by apoptosis and autophagy inhibitors in 6-OHDA-induced neuronal death. zVAD, 3-MA, and BafA were co-treated with 6-OHDA for 18 h. **a**–**d** LDH release analysis (**a**), cytosolic nucleosome analysis using ELISA (**b**), and FACS analysis using AnV and PI staining (**c**, **d**) after treatment of zVAD (100 μM), 3-MA (10 mM), or BafA (20 nM) with 6-OHDA (50 μM). **d** The analysis figure is representative data among triplicated experiments for the graph presented in **c**. The graph data are presented as the mean± S.E.M. with *p* values calculated using one-way ANOVA with Tukey post-hoc analysis (*n*=4 for Fig. 3a, b, *n*=3 for Fig. 3c). Statistical significance is indicated as *$p<0.05$ and **$p<0.01$ compared with the untreated control and #$p<0.05$ and ##$p<0.01$ compared with the 6-OHDA treatment alone

(PI$^+$). Thus, negative cells for both products are classified as viable (AnV$^-$/PI$^-$). In Fig. 3c, d, treatment of 6-OHDA decreased viable cell population (AnV$^-$/PI$^-$) and increased early apoptotic cell population (AnV$^+$/PI$^-$). Treatment with zVAD or 3-MA decreased the early apoptotic cell population (AnV$^+$/PI$^-$) compared to 6-OHDA alone. In contrast, treatment with BafA significantly increased early apoptotic (AnV$^+$/PI$^-$) and necrotic/late apoptotic (AnV$^-$/PI$^+$) cell population as well as decreased viable cell population (AnV$^-$/PI$^-$) compared to 6-OHDA alone. These results indicated that treatment of 6-OHDA led to apoptosis which was inhibited by treatment with zVAD or 3-MA. However, treatment with BafA increased the 6-OHDA-induced apoptosis and necrotic cell death.

Bafilomycin A1 Prevents the Clearance of Damaged Mitochondria and Induces Aberrant Oxygen Consumption

When cells were co-treated with BafA and 6-OHDA, the mitochondrial MTT reduction was recovered (Fig. 2a) but the apoptosis parameters were markedly increased (Fig. 2b and Fig. 3). To understand the discordance among the BafA effects, we evaluated the mitochondrial content. After treatment of 6-OHDA, mitochondrial cytochrome C oxidase subunit IV (COX IV) levels were decreased in a time-dependent manner (Fig. 4a, c). Co-treatment of zVAD or BafA with 6-OHDA inhibited the decrease of COX IV at 6 and 18 h compared to 6-OHDA alone, but 3-MA did not (Fig. 4b, d).

We next examined the effects of apoptosis and autophagy inhibitors on extracellular oxygen consumption after treatment with 6-OHDA. We monitored rates of extracellular oxygen consumption using oxygen-sensitive probe to measure cellular respiration and mitochondrial function. Extracellular oxygen consumption was reduced by 6-OHDA compared with untreated control. Treatment with BafA significantly increased the oxygen consumption compared to 6-OHDA alone from 8 h; however, zVAD and 3-MA had no effect (Fig. 4e). In staining with LysoTracker red, acidotropic probe, treatment with BafA induced loss of red fluorescence indicating lysosomal dysfunction (Fig. 4f). These observations indicated failure of mitochondrial clearance by lysosome because BafA is an inhibitor of autophagolysosome formation via the inhibition of lysosomal H$^+$-ATPase. Thus, these results suggested that BafA inhibited the loss of mitochondrial contents and remained mitochondrial respiration by 6-OHDA treatment. Finally, to identify the meaning of remained mitochondrial respiration by BafA co-treatment with 6-OHDA, we next confirm mitochondria status using Mitotracker Red and Green (Fig. 4g). MitoTracker green can stain all mitochondria and MitoTracker red only stains undamaged mitochondria.

6-OHDA decreased red-stained mitochondria and 3-MA or zVAD treatment reversed the staining. Interestingly, BafA treatment increased the loss of red-stained cells compared to 6-OHDA alone, which indicated increase of damaged mitochondria. Together with the results of Fig. 4, we concluded that 3-MA was not associated with mitochondrial clearance and zVAD inhibited the clearance without dysfunction of mitochondria. However, BafA prevented the clearance of damaged mitochondria by 6-OHDA and the mitochondria remained the respiration ability, which may result in aberrant mitochondrial respiration.

Bafilomycin A1 Does not Inhibit DHE-Sensitive ROS but Decreases DCF-DA-Sensitive ROS Below Basal Level in 6-OHDA-Treated Cells

To determine the relationship between the inhibitor of apoptosis or autophagy and the production of reactive oxygen species (ROS) in 6-OHDA-treated cells, we measured intracellular ROS production using dichlorodihydrofluorescein diacetate (DCF-DA) and dihydroethidium (DHE) dyes. Although there are debates as to which dye is more reactive to a specific form of ROS, DCF-DA can detect hydrogen peroxide (H_2O_2), and DHE is sensitive to superoxide ($O_2^{\circ-}$) [18, 19]. At the results, 6-OHDA increased DCF-DA fluorescence at 18 h (Fig. 5a, c), and treatment with zVAD, 3-MA, or BafA significantly inhibited the fluorescence (Fig. 5b, d). Next, the DHE fluorescence was significantly increased by 6-OHDA from 3 h (Fig. 5e, g), which was inhibited by zVAD and 3-MA but not BafA at 3 h (Fig. 5f, h). We observed that 6-OHDA induced DHE-sensitive ROS at early time period and DCF-DA-sensitive ROS at later time period, which well correlated with the previous concept that firstly generated ROS is superoxide and then is converted into hydrogen peroxide by superoxide dismutase (SOD). In our data, 6-OHDA-induced ROS were effectively lowered by treatment with zVAD or 3-MA. However, treatment with BafA only had reduced effect of DCF-DA-sensitive ROS.

To further investigate the effects of BafA on the 6-OHDA-induced ROS, we measured the two types of ROS through the time course from 1 to 18 h and compared 6-OHDA alone with co-treatment of BafA (Fig. 5i–l). Treatment with BafA showed a significant decrease in DCF-DA fluorescence compared to 6-OHDA alone from 3 h (Fig. 5i, k). Interestingly, this decrease showed below the basal level compared to the untreated control. Moreover, treatment with BafA did not reduce the DHE fluorescence at any time point, but rather induced transient increase at 6 h (Fig. 5j, k). Therefore, we concluded that BafA did not inhibit the production of DHE-sensitive ROS induced by 6-OHDA but markedly reduced DCF-DA-sensitive ROS.

Bafilomycin A1 Decreases the Level and Activity of Cu/Zn-SOD in 6-OHDA-Treated Cells

From the above data, we speculated that the effect of BafA on 6-OHDA-induced cell death might be associated with superoxide dismutase (SOD) status or activity because it was well

reported that the SOD converts from superoxide into hydrogen peroxide and our data showed that BafA co-treatment reduced DCF-DA even below basal level without reducing DHE fluorescence. Therefore, we examined the level and activity of Cu/Zn-SOD, MnSOD, and catalase (Fig. 6). In immunoblotting data, treatment with BafA significantly reduced
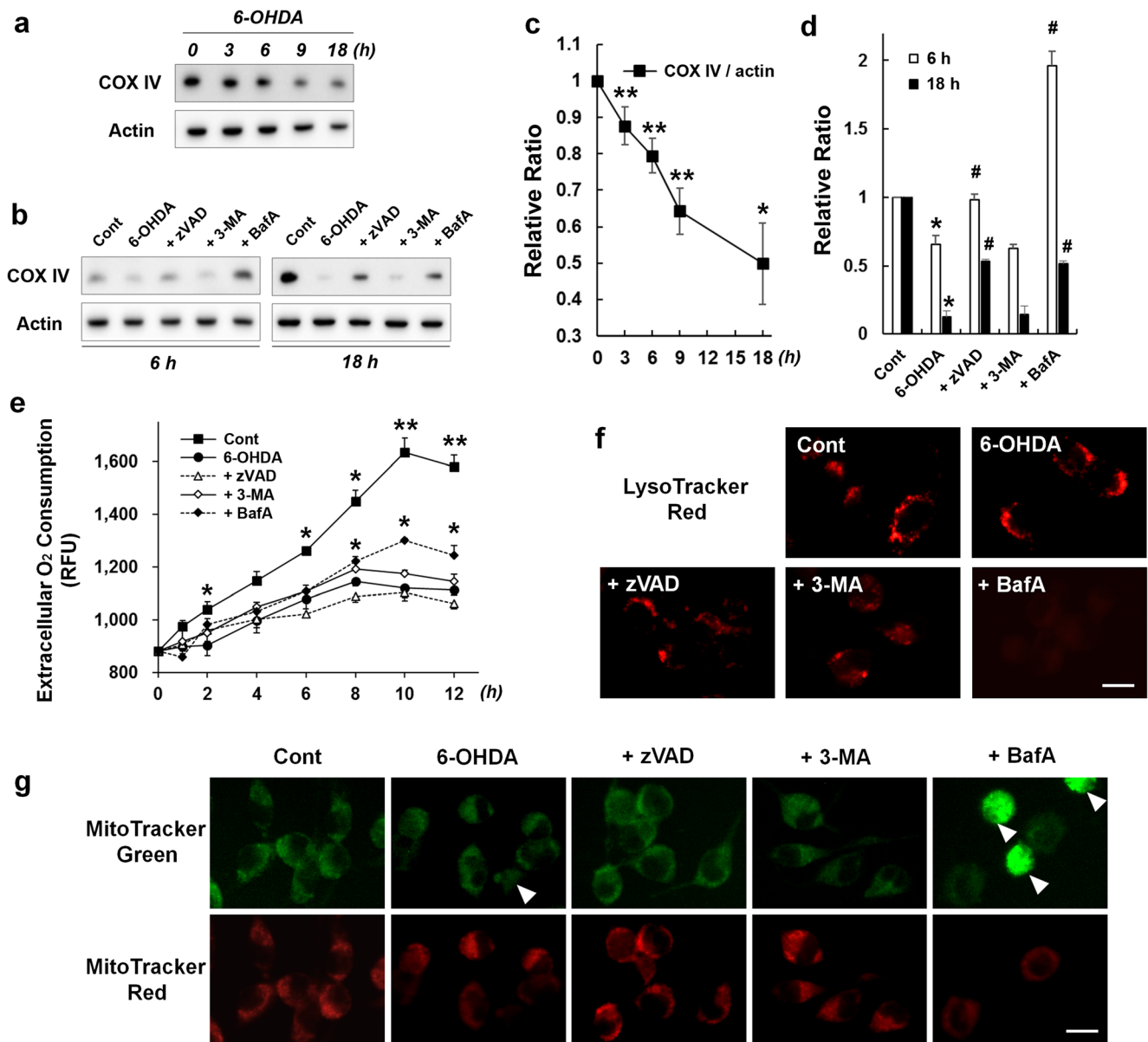

Fig. 4 Effects of apoptosis and autophagy inhibitors on 6-OHDA-induced change in mitochondrial content and respiration. **a** Time-dependent change of COX IV protein as a marker of mitochondria by 6-OHDA. **b** Protein levels of COX IV at 6 and 18 h after treatment of zVAD (100 μM), 3-MA (10 mM), or BafA (20 nM) with 6-OHDA (50 μM). **c, d** Densitometry data for COX IV/actin from **a** (**c**) and **b** (**d**). The ratio was normalized from the untreated control group. **e** Changes in extracellular oxygen consumptions at each time points (~12 h) after treatment of zVAD (100 μM), 3-MA (10 mM), or BafA (20 nM) with 6-OHDA (50 μM). **f** Representative images of LysoTracker signals. Cells

were co-treated with 6-OHDA and each inhibitor for 18 h and then stained with LysoTracker Red DND-99. **g** Representative images of MitoTracker signals. Cells were co-treated with 6-OHDA and each inhibitor for 18 h and then stained with MitoTracker green and red. The *arrowhead* represents the cell not stained with MitoTracker red. *Scale bar* represents 10 μm. The graph data are presented as the mean± S.E.M., with p values calculated using one-way ANOVA with Tukey post-hoc analysis ($n=3$). Statistical significance is indicated as *$p<0.05$ and **$p<0.01$ compared with the untreated control and #$p<0.05$ compared with the 6-OHDA treatment alone
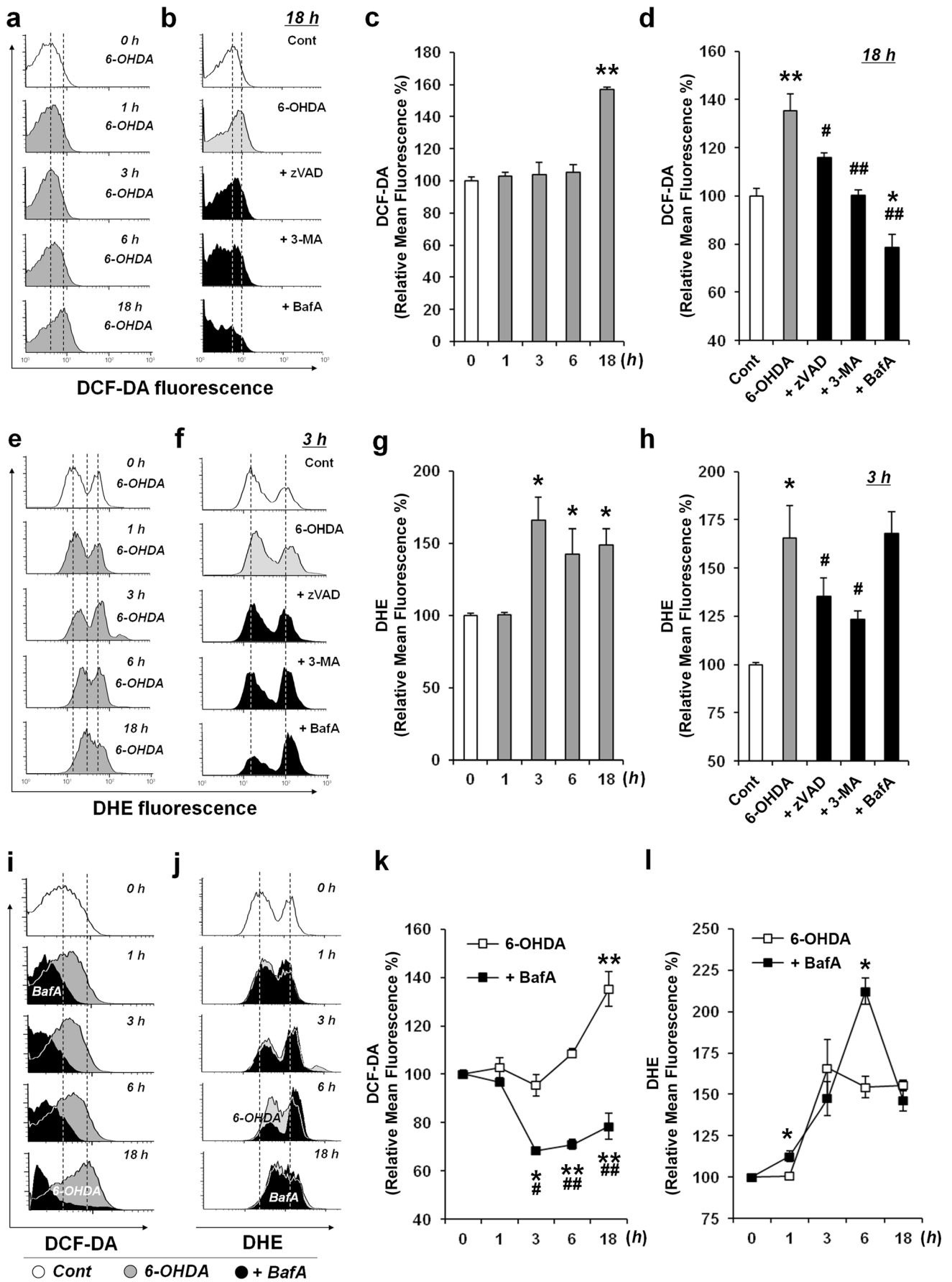
◄ **Fig. 5** Effects of apoptosis and autophagy inhibitors on 6-OHDA-induced formation of ROS. The DCF-DA and DHE fluorescence was measured using flow cytometry. **a–d** Change in DCF-DA fluorescence by apoptosis and autophagy inhibitors. **a, c** Time-dependent change in DCF-DA fluorescence after treatment of 6-OHDA for 18 h. **b, d** Changes in DCF-DA fluorescence induced by treatment of zVAD, 3-MA, or BafA with 6-OHDA treatment at 18 h. **a** and **b** are representative figures from triplicated experiments. **e–h** Change in DCF-DA fluorescence by apoptosis and autophagy inhibitors. **e, g** Time-dependent change in DCF-DA fluorescence after treatment of 6-OHDA for 18 h. **f, h** Changes in DCF-DA fluorescence induced by treatment of zVAD, 3-MA, or BafA with 6-OHDA treatment at 3 h. **e** and **f** are representative figures from triplicated experiments. **i–l** Time-dependent change in DCF-DA (**i, k**) and DHE (**j, l**) fluorescence after 6-OHDA treatment with or without BafA for 18 h. **i** and **j** are representative figures from triplicated experiments. The graph data are presented as the mean±S.E.M. with p values calculated using one-way ANOVA with Tukey post-hoc analysis ($n=3$). Statistical significance is indicated as *$p<0.05$ and **$p<0.01$ compared with the untreated control and #$p<0.05$ and ##$p<0.01$ compared with 6-OHDA treatment alone

the level of Cu/Zn-SOD compared with 6-OHDA alone at 6 and 18 h but treatment with zVAD or 3MA did not. The level of MnSOD was more increased by treatment with BafA than with 6-OHDA alone at 6 h. The level of catalase was slightly increased by 6-OHDA compared to the control at 18 h, which was not altered by treatment with the inhibitors (Fig. 6a–c).

Total SOD activity was increased by 3-MA co-treatment and was decreased by BafA compared to 6-OHDA alone at 6 and 18 h (Fig. 6d, e). MnSOD activity was also increased by the treatment with 3-MA compared with 6-OHDA alone at each time point but was not changed by the treatment with zVAD or BafA. At 18 h, Cu/Zn-SOD activity was decreased by 6-OHDA, which was more significantly lowered by treatment with BafA compared to 6-OHDA treatment alone (Fig. 6d, e). Catalase activity was not changed by 6-OHDA and the inhibitors (Fig. 6f). We concluded that treatment with
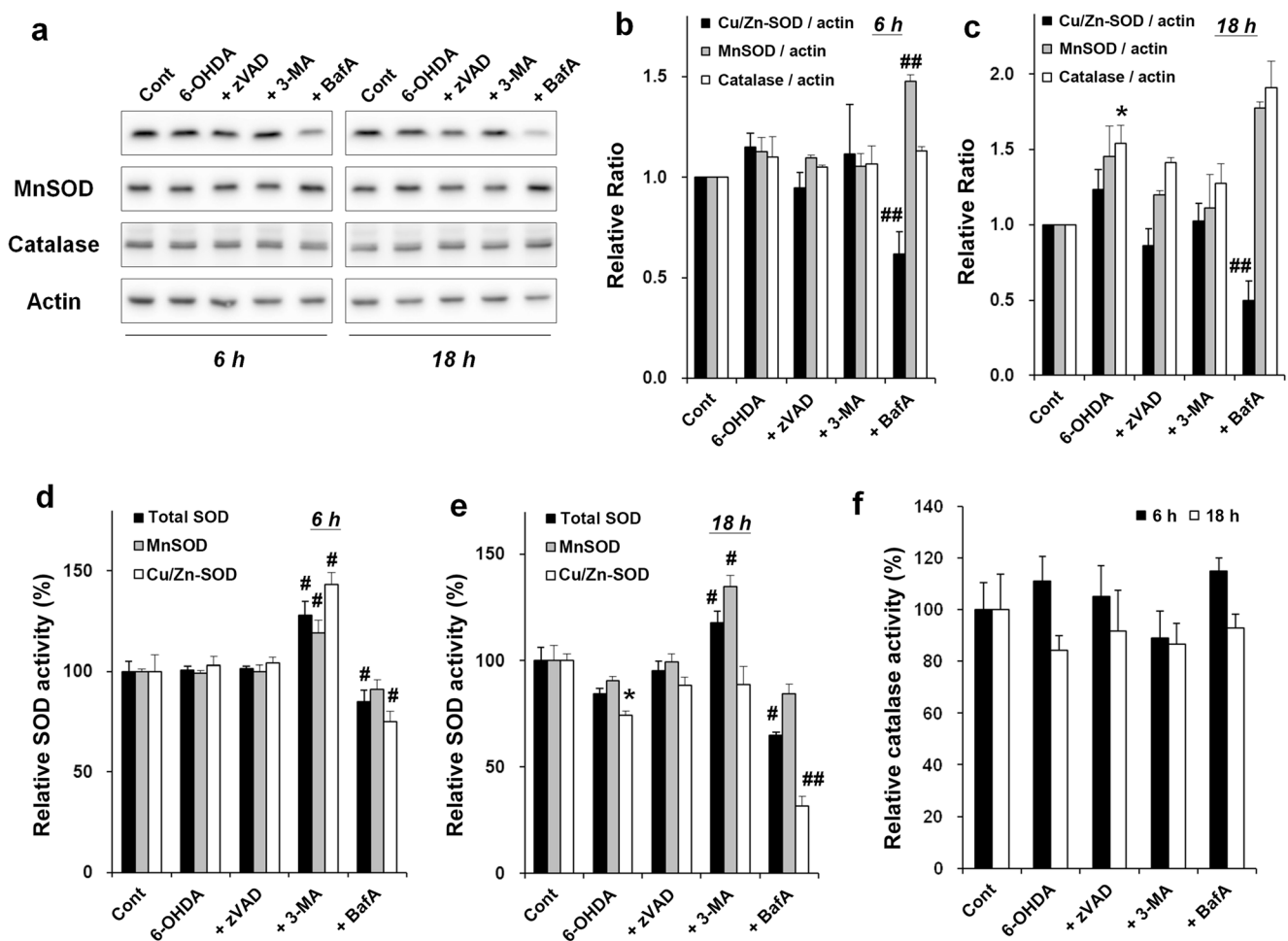

Fig. 6 Effects of apoptosis and autophagy inhibitors on 6-OHDA-induced decrease in Cu/Zn-SOD level and activity. **a** Changes in Cu/Zn-SOD, MnSOD, and catalase protein level at 6 and 18 h evaluated using immunoblots after treatment of zVAD (100 μM), 3-MA (10 mM), or BafA (20 nM) with 6-OHDA (50 μM). **b, c** Densitometry data for Cu/Zn-SOD, MnSOD, or catalase per actin at 6 h (**b**) and 18 h (**c**) from **a**. The ratio was normalized from the untreated control group. **d, e** Relative activities of total SOD, MnSOD, and Cu/Zn-SOD after treatment of 6-OHDA with or without the inhibitors. **f** Relative activity of catalase after treatment of 6-OHDA with or without the inhibitors. The ratio was normalized from the untreated control group. The graph data are presented as the mean±S.E.M., with p values calculated using one-way ANOVA with Tukey post-hoc analysis ($n=3$ for **b**, **c**; $n=4$ for **e**, **f**). Statistical significance is indicated as *$p<0.05$ and **$p<0.01$ compared with the untreated control and #$p<0.05$ and ##$p<0.01$ compared with the 6-OHDA treatment alone

BafA decreased the protein level of Cu/Zn-SOD, which could lead to the loss of Cu/Zn-SOD activity with the consequent decrease of total SOD activity.

Discussion

6-OHDA, a neurotoxin among parkinsonian mimetics, induces lesions of dopaminergic neurons and is commonly used to develop experimental models for Parkinson's disease; however, little is known regarding the underlying mechanism of 6-OHDA-induced neuronal cell death [7, 10]. According to recent reports, 6-OHDA induced caspase-dependent apoptosis as well as autophagy-related cell death [20, 21]. However, the exact relationship between apoptosis and autophagy in 6-OHDA-induced death is not well defined. Therefore, in the present study, we focused on elucidating the detailed mechanism underlying 6-OHDA-induced neuronal cell death. We examined the participation of apoptosis and autophagy in 6-OHDA-induced cell death with zVAD (pan-caspase inhibitor) and 3-MA and BafA (autophagy inhibitors). In addition, we investigated the effects of apoptosis and autophagy inhibitors on 6-OHDA-mediated reactive oxygen species production and loss of mitochondria.

A high efficiency of autophagy flux is indicated by an increased level of conversion from LC3-I to LC3-II and a decreased level of p62 protein. Additionally, the inhibition of autophagolysosome formation from autophagosome can be also represented by LC3-II and p62 accumulation [16, 17]. We observed that 6-OHDA induces early autophagy induction (from 3 h) through LC3-II conversion and later inhibits the autophagic flux (from 9 h), which involves the accumulation of LC3-II and p62 (Fig. 1). Caspase-3 activation occurred at 18 h by 6-OHDA after the decrease of autophagy flux. This indicated that the inhibition of autophagy flux may lead to apoptosis activation (Fig. 2). Thus, these results were further confirmed by treatment with apoptosis or autophagy inhibitors. 3-MA, an autophagy inhibitor at the early or initiation phase, inhibited the activation of caspase-3 and inductions of other apoptosis markers by 6-OHDA (Figs. 2b–d and 3b–d), and co-treatment with zVAD did not affect the accumulation of LC3-II (Fig. 2b–d), which indicated that autophagy signal was upstream of caspase-dependent apoptosis. In addition, co-treatment with BafA, an autophagy inhibitor at a later phase or inhibitor of autophagolysosome formation, exacerbated the inhibition of the autophagy flux by 6-OHDA showing increases of p62 accumulation, LC3-II conversion, and mCherry/GFP-LC3 co-localization (Fig. 2b–g). It was thought that the inhibition of autophagy flux was not fully induced by 6-OHDA alone, because BafA addition enhanced the inhibition of the flux. Therefore, we concluded that the inhibition of autophagic flux by 6-OHDA may be a causative

factor of the caspase-dependent apoptosis. These results also indicate that the inhibition of autophagy induction by such as 3-MA can suppress apoptosis activation, but the inhibition of fusion between autophagosome and lysosome by BafA causes aggravation of 6-OHDA-induced cell death.

In MTT reduction assay, the co-treatment with 3-MA showed a greater decrease and BafA increased the reduction compared with 6-OHDA alone (Fig. 2a). On the other hand, LDH release was significantly increased by co-treatment with BafA compared with 6-OHDA alone. Increases of LDH release and cytosolic nucleosome through 6-OHDA were inhibited by co-treatment with 3-MA or zVAD (Fig. 3a, b). Next, through FACS analysis after staining with AnV and PI, we obtained a similar result with LDH release and cytosolic nucleosome. These data indicated that MTT analysis for mitochondrial reduction activity showed opposite pattern compared to other parameters for cell death. Thus, we hypothesized that BafA with 6-OHDA may induce mitochondrial abnormality and next examined the mitochondrial content using immunoblot analysis of COX IV, which can represent the loss of mitochondria induced by 6-OHDA. Co-treatment with zVAD or BafA inhibited the mitochondrial loss but not with 3-MA (Fig. 4a–d). According to recent reports, parkinsonian mimetics such as 6-OHDA or MPP$^+$ induced mitochondrial clearance via mitophagy [22, 23]. Generally, mitophagy and macroautophagy can be well inhibited by the autophagy inhibitors, 3-MA and BafA [24, 25]. Our data showed the degradation or clearance of mitochondria by 6-OHDA which was suppressed by BafA. However, co-treatment with 3-MA did not reduce the mitochondrial loss, which indicated inhibitory effect of 3-MA on mitophagy in our system but may not match with the above previous reports [24, 25].

A recent review indicates variants of mitochondrial autophagy, which involves type 1 (primarily via nutrient deprivation), type 2 (via mitochondrial damage such as photodamage), and type 3 mitophagy (occurring with microautophagy). This classification can be additionally defined through response to chemical inhibition: phosphatidyl inositol 3-phosphate kinase (PI3K) inhibition with 3-MA or wortmannin blocks type 1 but not type 2 mitophagic sequestration [26]. The initiating stimuli for type 2 mitophagy are usually mitochondrial depolarization by inducer such as photodamage [26]. Considering this report, our setting appears to be similar to type 2 mitophagy because 6-OHDA can depolarize the mitochondrial membrane [7, 10, 11]. In addition, we found that zVAD as well as BafA inhibited the mitochondrial loss induced by 6-OHDA. In our results, zVAD could not inhibit the mitophagy process itself and instead may prevent mitochondrial clearance because there were reports that zVAD maintains mitophagy process but inhibits mitochondrial clearance via lysosome in the cellular stress such as UV-irradiated mitochondrial damage or starvation-induced apoptosis [27, 28]. It was also reported that high dose
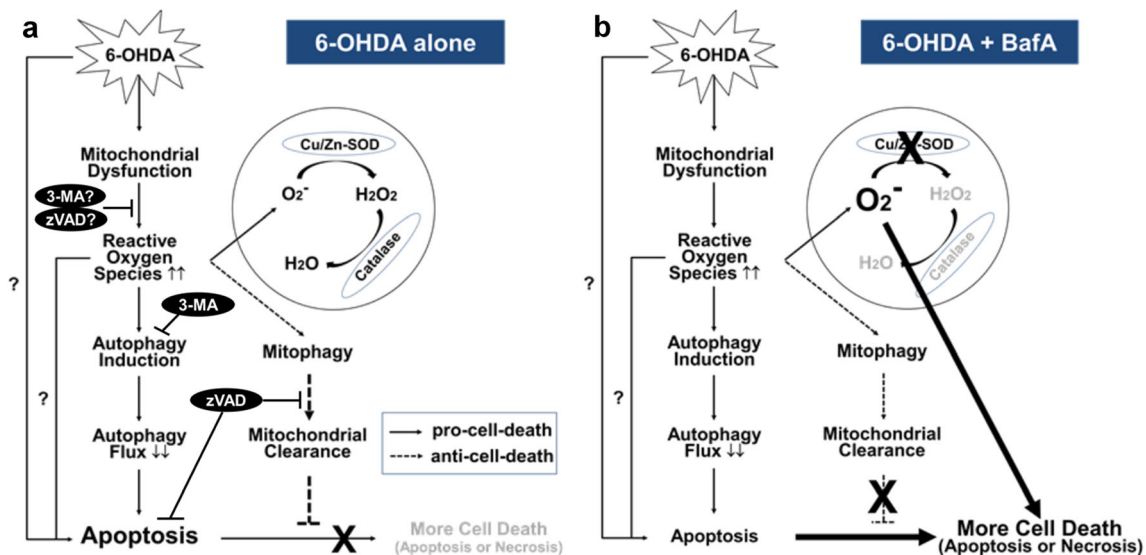
Fig. 7 Schematic model for 6-OHDA-induced cell death. **a** 6-OHDA-induced autophagy and subsequent apoptosis. 6-ODHA induces apoptosis through ROS production, autophagy induction, autophagy flux inhibition, and final apoptosis sequentially (pro-cell death pathway). In addition, 6-OHDA induces mitochondrial clearance, which may be protective and can prevent more apoptosis or necrosis via ROS production from damaged mitochondria (anti-cell death pathway). 3-MA blocked pro-cell death pathway at both steps of ROS production and autophagy induction. zVAD separately blocks ROS production and mitochondrial clearance. **b** BafA effects in the 6-OHDA-mediated cell death. BafA blocks clearance of damaged mitochondria, thereby resulting in constant ROS production. Moreover, BafA inhibits Cu/Zn-SOD activity, which leads to accumulation of superoxide, most toxic ROS

of zVAD over 50 μM suppresses the activation of lysosomal enzymes by various stimuli but not low dose [29, 30].

Next, in our data, BafA showed similar effects with zVAD for mitochondrial clearance, but uncleared mitochondria by BafA seemed to be abnormal. The uncleared mitochondria showed more consumption of extracellular oxygen by BafA compared with 6-OHDA alone, but not by zVAD (Fig. 4e). These changes were also confirmed with co-localization of MitoTracker green and red, which can visualize damaged mitochondria through the loss of red signal. We found no stained red signal by BafA co-treatment compared with 6-ODHA alone indicating BafA-induced mitochondrial damage (Fig. 4g). In other results of BafA, the co-treatment with BafA increased the extent of cell death, which may involve apoptosis and/or necrosis, because the level of caspase-3 cleavage, LDH release, and AnV$^+$/PI$^-$ and AnV$^-$/PI$^+$ population in FACS analysis was more increased by co-treatment of BafA (Figs. 2 and 3). Moreover, the co-treatment of BafA increased the MTT reduction (Fig. 2a) and extracellular oxygen consumption (Fig. 4e), which was correlated with the inhibition of mitochondrial loss (Fig. 4a–d), and mitochondrial and lysosomal dysfunction (Fig. 4f–g). Previous study reported that BafA co-treatment aggravated cell death and ROS formation in *t*-butylhydroperoxide-treated hepatocytes [31]. Therefore, we concluded that 6-OHDA with BafA induced both mitochondrial damage and aberrant respiration. We next studied the intracellular ROS status because the abnormal mitochondrial respiration was closely correlated with ROS production.

To measure intracellular ROS, we used two types of ROS sensitive dyes, DCF-DA and DHE. Although there are debates which dye is more reactive to a specific form of ROS, DCF-DA can detect hydrogen peroxide and DHE is sensitive to superoxide [18, 19]. We observed that 6-OHDA induced DHE fluorescence from 3 h and DCF-DA fluorescence at 18 h, indicating early superoxide production and late hydrogen peroxide formation (Fig. 5). At each peak time of fluorescence, treatment with 3-MA or zVAD significantly inhibited ROS production compared with 6-OHDA alone. Co-treatment with BafA blocked DCF-DA fluorescence but not DHE fluorescence (Fig. 5d, h). In our data, it seems that both 3-MA and zVAD could directly suppress intracellular ROS formation. It was reported that 3-MA decreased ROS generation in sodium nitroprusside-induced apoptosis of PC12 cells or hydroquinone-induced oxidative damage of retinal cells [32, 33]. zVAD also inhibits ROS generation in TNFα-stimulated neutrophil or caspase-3/truncated BH3-interacting domain death agonist (tBID)-mediated apoptosis [34, 35]. Although it is still debatable that these inhibitions of ROS production by 3-MA or zVAD are caused from higher concentration [35, 36], we concluded that 3-MA and zVAD could inhibit 6-OHDA-induced superoxide and hydrogen peroxide production.

Finally, we focused on the effect of BafA on ROS production. In this study, co-treatment with BafA did not reduce or transiently increased superoxide and decreased hydrogen peroxide compared with the 6-OHDA

treatment alone (Fig. 5i–l). Interestingly, BafA co-treatment decreased hydrogen peroxide to below the basal level compared with the untreated control. It was previously reported that SOD enzymes detoxified super-oxide to hydrogen peroxide and catalase enzyme cata-lyzes the peroxide [37]. Thus, we next examined the levels and activities of intracellular SODs and catalase. We found that the activity of Cu/Zn-SOD was signifi-cantly decreased by treatment with BafA (Fig. 6). The decrease of activity appeared to be caused by the de-creased expression of Cu/Zn-SOD because the extent of decrease in expression and activity was similar in the present study. In this regard, we thought that the de-crease of Cu/Zn-SOD level was not caused at the tran-scription level because the transcriptional regulation need for relatively long time during the process (more than 6~12 h). Moreover, reports for the transcriptional modulation of Cu/Zn-SOD have been relatively rare [38]. Therefore, we postulated that the decrease of Cu/Zn-SOD activity and expression was caused by degra-dation or stability change of Cu/Zn-SOD. According to previous reports, Cu/Zn-SOD activity can be regulated by a change of maturation by oxygenation and/or by change of binding with a specific chaperone such as copper chaperone for SOD1 (CCS) [39, 40]. In addition, Cu/Zn-SOD can be modified by ubiquitination or sumoylation, which may be associated with the proteasomal degradation of Cu/Zn-SOD [41–43]. To-gether with these reports, our data suggested that treat-ment with BafA and 6-OHDA decreased the stability and activity of Cu/Zn-SOD. This loss may maintain more accumulation of toxic superoxide without the de-toxification into the lesser toxic hydrogen peroxide.

Altogether, treatment of bafilomycin A1 exacerbated neu-ronal apoptosis via the dysfunction of Cu/Zn-SOD and the inhibition of mitochondrial clearance in 6-OHDA-treated neu-ronal cells. In this study, we performed several approaches demonstrating relationship among oxidative stress, autopha-gy, and apoptosis. We examined changes of various markers for oxidative stress, autophagy, and apoptosis and confirmed these changes using inhibitors of autophagy and apoptosis. 3-MA treatment inhibited 6-OHDA-induced autophagy initia-tion and later induction of apoptosis without affecting mito-chondrial clearance. zVAD treatment blocked the ROS pro-duction and the mitochondrial clearance. Finally, the treatment with BafA blocked the mitochondrial clearance and led to the dysfunction of Cu/Zn-SOD activity. From these results, we suggested that 6-OHDA-mediated neuronal cell death in-volves induction of autophagy, subsequent inhibition of the autophagy flux, and resultant apoptosis. Additionally, 6-OHDA induced mitochondrial clearance, which could be a protective effect to prevent further necrosis or apoptosis via maintaining superoxide without detoxification into hydrogen

peroxide (Fig. 7). Therefore, the present study suggests that the interaction of oxidative stress, autophagy, and apoptosis is a major contributing factor in 6-OHDA-mediated neuronal death and provides an understanding of the cellular mecha-nisms in PD pathogenesis.

Conflict of Interest The authors declare that they have no conflict of interests.

References

1. Shults CW (2003) Treatments of Parkinson disease: circa 2003. Arch Neurol 60:1680–1684. doi:10.1001/archneur.60.12.1680
2. Eriksen JL, Wszolek Z, Petrucelli L (2005) Molecular pathogenesis of Parkinson disease. Arch Neurol 62:353–357. doi:10.1001/archneur.62.3.353
3. Ross CA, Smith WW (2007) Gene-environment interactions in Parkinson's disease. Parkinsonism Relat Disord 13:S309–S315. doi:10.1016/S1353-8020(08)70022-1
4. Henchcliffe C, Beal MF (2008) Mitochondrial biology and oxidative stress in Parkinson disease pathogenesis. Nat Clin Pract Neurol 4:600–609. doi:10.1038/ncpneuro0924
5. Zabel C, Nguyen HP, Hin SC, Hartl D, Mao L, Klose J (2010) Proteasome and oxidative phosphorylation changes may explain why aging is a risk factor for neurodegenerative disorders. J Proteomics 73:2230–2238. doi:10.1016/j.jprot.2010.08.008
6. Cheung ZH, Ip NY (2009) The emerging role of autophagy in Parkinson's disease. Mol Brain 16:2–29. doi:10.1186/1756-6606-2-29
7. Blandini F, Armentero MT, Martignoni E (2008) The 6-hydroxydopamine model: news from the past. Parkinsonism Relat Disord 14:S124–S129. doi:10.1016/j.parkreldis.2008.04.015
8. Chandra J, Samali A, Orrenius S (2000) Triggering and modulation of apoptosis by oxidative stress. Free Radic Biol Med 29:323–333
9. Zhou C, Huang Y, Przedborski S (2008) Oxidative stress in Parkinson's disease: a mechanism of pathogenic and therapeutic sig-nificance. Ann N Y Acad Sci 1147:93–104. doi:10.1196/annals.1427.023
10. Blum D, Torch S, Lambeng N, Nissou M, Benabid AL, Sadoul R, Verna JM (2001) Molecular pathways involved in the neurotoxicity of 6-OHDA, dopamine and MPTP: contribution to the apoptotic theory in Parkinson's disease. Prog Neurobiol 65:135–172
11. Venderova K, Park DS (2012) Programmed cell death in Parkinson's disease. Cold Spring Harb Perspect Med 2:a009365. doi:10.1101/cshperspect.a009365
12. Yang Q, Mao Z (2010) Parkinson disease: a role for autophagy? Neuroscientist 16:335–341. doi:10.1177/1073858409357118
13. Dagda RK, Zhu J, Kulich SM, Chu CT (2008) Mitochondrially lo-calized ERK2 regulates mitophagy and autophagic cell stress: impli-cations for Parkinson's disease. Autophagy 4:770–782
14. Jang BG, Choi BY, Kim JH, Kim MJ, Sohn M, Suh SW (2013) Impairment of autophagic flux promotes glucose reperfusion-induced neuro2A cell death after glucose deprivation. PLoS One 8:e76466. doi:10.1371/journal.pone.0076466

15. Liu Y, Wong TP, Aarts M, Rooyakkers A, Liu L, Lai TW, Wu DC, Lu J, Tymianski M, Craig AM, Wang YT (2007) NMDA receptor subunits have differential roles in mediating excitotoxic neuronal death both in vitro and in vivo. J Neurosci 27:2846–2857. doi:10.1523/JNEUROSCI. 0116-07.2007

16. Puissant A, Fenouille N, Auberger P (2012) When autophagy meets cancer through p62/SQSTM1. Am J Cancer Res 2:397–413

17. Klionsky DJ, Abdalla FC, Abeliovich H et al (2012) Guidelines for the use and interpretation of assays for monitoring autophagy. Autophagy 8:445–544

18. Zhao H, Kalivendi S, Zhang H, Joseph J, Nithipatikom K, Vasquez-Vivar J, Kalyanaraman B (2003) Superoxide reacts with hydroethidine but forms a fluorescent product that is distinctly different from ethidium: potential implications in intracellular fluorescence detection of superoxide. Free Radic Biol Med 34:1359–1368

19. Gomes A, Fernandes E, Lima JL (2005) Fluorescence probes used for detection of reactive oxygen species. J Biochem Biophys Methods 65:45–80. doi:10.1016/j.jbbm.2005.10.003

20. Arsikin K, Kravic-Stevovic T, Jovanovic M, Ristic B, Tovilovic G, Zogovic N, Bumbasirevic V, Trajkovic V, Harhaji-Trajkovic L (2012) Autophagy-dependent and -independent involvement of AMP-activated protein kinase in 6-hydroxydopamine toxicity to SH-SY5Y neuroblastoma cells. Biochim Biophys Acta 1822:1826–1836. doi:10.1016/j.bbadis.2012.08.006

21. Ossola B, Lantto TA, Puttonen KA, Tuominen RK, Raasmaja A, Mannisto PT (2012) Minocycline protects SH-SY5Y cells from 6-hydroxydopamine by inhibiting both caspase-dependent and -independent programmed cell death. J Neurosci Res 90:682–690. doi:10.1002/jnr.22791

22. Chu CT, Zhu J, Dagda R (2007) Beclin 1-independent pathway of damage-induced mitophagy and autophagic stress: implications for neurodegeneration and cell death. Autophagy 3:663–666

23. Dagda RK, Zhu J, Kulich SM, Chu CT (2008) Mitochondrially localized ERK2 regulates mitophagy and autophagic cell stress: implications for Parkinson's disease. Autophagy 4:770–782

24. Van Humbeeck C, Cornelissen T, Hofkens H, Mandemakers W, Gevaert K, De Strooper B, Vandenberghe W (2011) Parkin interacts with Ambra1 to induce mitophagy. J Neurosci 31:10249–10261. doi:10.1523/JNEUROSCI. 1917-11.2011

25. Kim SJ, Syed GH, Siddiqui A (2013) Hepatitis C virus induces the mitochondrial translocation of Parkin and subsequent mitophagy. PLoS Pathog 9:e1003285. doi:10.1371/journal.ppat.1003285

26. Lemasters JJ (2014) Variants of mitochondrial autophagy: types 1 and 2 mitophagy and micromitophagy (type 3). Redox Biol 2:749–754. doi:10.1016/j.redox.2014.06.004

27. Hailey DW, Rambold AS, Satpute-Krishnan P, Mitra K, Sougrat R, Kim PK, Lippincott-Schwartz J (2010) Mitochondria supply membranes for autophagosome biogenesis during starvation. Cell 141:656–667. doi:10.1016/j.cell.2010.04.009

28. Parone PA, James DI, Da Cruz S, Mattenberger Y, Donzé O, Barja F, Martinou JC (2006) Inhibiting the mitochondrial fission machinery does not prevent Bax/Bak-dependent apoptosis. Mol Cell Biol 26:7397–7408. doi:10.1128/MCB. 02282-05

29. Schotte P, Declercq W, Van Huffel S, Vandenabeele P, Beyaert R (1999) Non-specific effects of methyl ketone peptide inhibitors of caspases. FEBS Lett 442:117–121

30. Nylandsted J, Gyrd-Hansen M, Danielewicz A, Fehrenbacher N, Lademann U, Høyer-Hansen M, Weber E, Multhoff G, Rohde M, Jäättelä M (2004) Heat shock protein 70 promotes cell survival by inhibiting lysosomal membrane permeabilization. J Exp Med 200:425–435. doi:10.1084/jem.20040531

31. Uchiyama A, Kim JS, Kon K, Jaeschke H, Ikejima K, Watanabe S, Lemasters JJ (2008) Translocation of iron from lysosomes into mitochondria is a key event during oxidative stress-induced hepatocellular injury. Hepatology 48:1644–1654. doi:10.1002/hep.22498

32. Liu B, Yang P, Ye Y, Zhou Y, Li L, Tashiro S, Onodera S, Ikejima T (2011) Role of ROS in the protective effect of silibinin on sodium nitroprusside-induced apoptosis in rat pheochromocytoma PC12 cells. Free Radic Res 45:835–847. doi:10.3109/10715762.2011.580343

33. Ramírez C, Pham K, Franco MF, Chwa M, Limb A, Kuppermann BD, Kenney MC (2013) Hydroquinone induces oxidative and mitochondrial damage to human retinal Müller cells (MIO-M1). Neurotoxicology 39:102–108. doi:10.1016/j.neuro.2013.08.004

34. Ricci JE, Gottlieb RA, Green DR (2003) Caspase-mediated loss of mitochondrial function and generation of reactive oxygen species during apoptosis. J Cell Biol 160:65–75. doi:10.1083/jcb.200208089

35. Cowburn AS, White JF, Deighton J, Walmsley SR, Chilvers ER (2005) z-VAD-fmk augmentation of TNF alpha-stimulated neutrophil apoptosis is compound specific and does not involve the generation of reactive oxygen species. Blood 105:2970–2972. doi:10.1182/blood-2004-07-2870

36. Rikiishi H (2012) Novel insights into the interplay between apoptosis and autophagy. Int J Cell Biol 2012:317645. doi:10.1155/2012/317645

37. Li H, Horke S, Förstermann U (2013) Oxidative stress in vascular disease and its pharmacological prevention. Trends Pharmacol Sci 34:313–319. doi:10.1016/j.tips.2013.03.007

38. Miao L, St Clair DK (2009) Regulation of superoxide dismutase genes: implications in disease. Free Radic Biol Med 47:344–356. doi:10.1016/j.freeradbiomed.2009.05.018

39. Furukawa Y, Torres AS, O'Halloran TV (2004) Oxygen-induced maturation of SOD1: a key role for disulfide formation by the copper chaperone CCS. EMBO J 23:2872–2881. doi:10.1038/sj.emboj.7600276

40. Banci L, Bertini I, Cantini F, Kozyreva T, Massagni C, Palumaa P, Rubino JT, Zovo K (2012) Human superoxide dismutase 1 (hSOD1) maturation through interaction with human copper chaperone for SOD1 (hCCS). Proc Natl Acad Sci U S A 109:13555–13660. doi:10.1073/pnas.1207493109

41. Di Noto L, Whitson LJ, Cao X, Hart PJ, Levine RL (2005) Proteasomal degradation of mutant superoxide dismutases linked to amyotrophic lateral sclerosis. J Biol Chem 280:39907–39913. doi:10.1074/jbc.M506247200

42. Fei E, Jia N, Yan M, Ying Z, Sun Q, Wang H, Zhang T, Ma X, Ding H, Yao X, Shi Y, Wang G (2006) SUMO-1 modification increases human SOD1 stability and aggregation. Biochem Biophys Res Commun 347:406–412. doi:10.1016/j.bbrc.2006.06.092

43. Ezzi SA, Urushitani M, Julien JP (2007) Wild-type superoxide dismutase acquires binding and toxic properties of ALS-linked mutant forms through oxidation. J Neurochem 102:170–178. doi:10.1111/j.1471-4159.2007.04531.x